2019

Automated Polarization-dependent Multidimensional Coherent Spectroscopy Phased Using Transient Absorption

J. K. Wahlstrand

G. M. Wernsing

J. Paul

A. D. Bristow

Research Article | Vol. 27, No. 22 / 28 October 2019 / Optics Express 31790
Optics EXPRESS

Automated polarization-dependent multidimensional coherent spectroscopy phased using transient absorption

J. K. WAHLSTRAND,[1,4] G. M. WERNSING,[1,2] J. PAUL,[1,3] AND A. D. BRISTOW[1,3,5]

[1]Nanoscale Device Characterization Division, National Institute of Standards and Technology, Gaithersburg, MD 20899, USA
[2]Electrical and Computer Engineering, Worcester Polytechnic Institute, Worcester, MA 01609, USA
[3]Department of Physics and Astronomy, West Virginia University, Morgantown, WV 26506-6315, USA
[4]jared.wahlstrand@nist.gov
[5]alan.bristow@mail.wvu.edu

Abstract: An experimental apparatus is described for multidimensional optical spectroscopy with fully automated polarization control, based on liquid crystal variable retarders. Polarization dependence of rephasing two-dimensional coherent spectra are measured in a single scan, with absolute phasing performed for all polarization configurations through a single automated auxiliary measurement at the beginning of the scan. A factor of three improvement in acquisition time is demonstrated, compared to the apparatus without automated polarization control. Results are presented for a GaAs quantum well sample and an InGaAs quantum well embedded in a microcavity.

1. Introduction

Two-dimensional optical coherent spectroscopy techniques are typically three-pulse measurements of the complex third-order nonlinear susceptibility through the four-wave mixing (FWM) response [1]. Microscopic variations in the local electronic environment [2–5] or many-body effects [6–9] cause subtle changes in the frequency-dependent third-order nonlinear susceptibility. Dependence on multi-pulse polarization configurations provides even more information by suppressing or enhancing particular features through the use of selection rules. Multidimensional coherent spectroscopy techniques at optical frequencies have been in development for nearly two decades [1,10,11], but measuring the full polarization-dependent complex susceptibility remains an arduous task.

The amplitude of the complex multi- or two-dimensional coherent spectrum (2DCS) contains information about broadening and coupling mechanisms of and between transitions. The only requirement to extract the amplitude spectrum is to have stable relative phases. However, much more information can be gleaned from the phase of the 2D spectrum. Unless the phase of the FWM with respect to the excitation pulses is known, the 2D spectrum is multiplied by an overall unknown phase. This phase is typically determined by comparing a slice of the complex FWM spectrum to the shape of the spectrally resolved transient absorption (SRTA) [1] or by an all-optical method that accounts for all unknown phase ambiguities [12]. The SRTA based technique only works for certain polarization configurations, while the all-optical method fails when the sample is too dispersive.

In this article, it is demonstrated that by using liquid-crystal variable retarders (VRs) to control the polarization of the excitation and emission pulses in 2DCS, spectra for multiple polarization combinations can be captured in a single scan of the delay stages. Because the relative phase imparted on the pulses by the VRs is calculable, we can phase the collinearly polarized spectrum

#375576 https://doi.org/10.1364/OE.27.031790
Journal © 2019 Received 19 Aug 2019; revised 30 Sep 2019; accepted 30 Sep 2019; published 17 Oct 2019

Optics EXPRESS

by the SRTA method and apply that phase to all other data regardless of their polarization configuration. Furthermore, liquid crystal based polarization control dramatically speeds up data acquisition in our actively stabilized, mechanical stage based scheme, because the polarization can be modulated much faster than the time step can be changed.

The technique is demonstrated on two semiconductor systems: (1) a 4-period GaAs-based multiple quantum well (QW) for direct comparison to previously published results [6,13], and (2) a QW embedded in a semiconductor microcavity (MC) with a moderate negative detuning to produce distinguishable exciton-like and cavity-like modes of the two exciton-polariton branches. The amplitude spectrum of this MC sample can be compared to previous work [14], but phased 2DCS spectra for any polarization, to the best of our knowledge, have not been reported in a MC sample.

2. Experiment

The experimental scheme is based on a Multidimensional Optical Nonlinear SpecTRometer (MONSTR) [15], which uses active stabilization to produce four phase-stable pulses from a single pulse emitted by a mode-locked Ti:sapphire oscillator. The pulses are emitted at a repetition rate of 76 MHz with 120 fs duration and centered near 800 nm. The MONSTR arranges the four pulses in a box geometry with arbitrary control of their respective delay times, while maintaining phase stability between them by employing active feedback using piezoelectric transducers referenced with a HeNe metrology laser. Figure 1 shows a schematic diagram of the experimental setup downstream from the MONSTR. Pulses labelled A, B, and C excite the sample. The fourth pulse is split into *tracer* (transmitted) and *reference* (reflected) pulses. The tracer pulse is used for alignment and also acts as the probe for measurement of SRTA, but is blocked during 2D scans. The FWM is emitted along the direction of the tracer, corresponding to the phase matching condition $-\mathbf{k}_A + \mathbf{k}_B + \mathbf{k}_C$, and is combined with the reference pulse and sent to a spectrometer. Interference between the reference pulse and FWM emission results in spectral fringes, which are analyzed to find the FWM amplitude and phase [16]. For the rephasing scan presented here, the order of excitation pulses is ABC, and the complex FWM emission is captured as a function of delay time τ between the A and B pulses, while keeping the B-C and C-Reference delay times fixed.

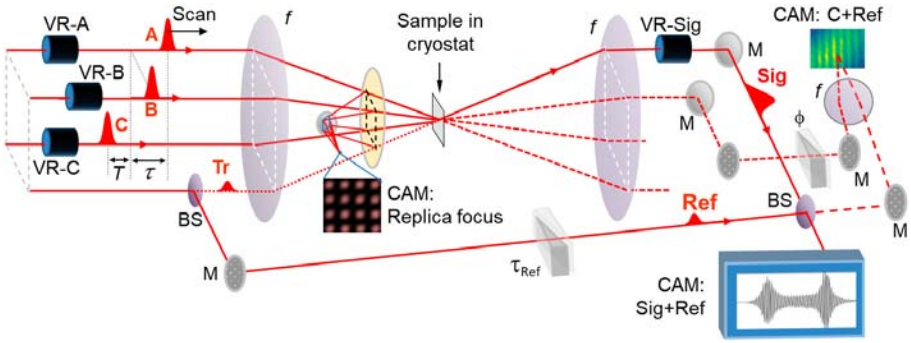

Fig. 1. Diagram of the experimental setup, showing the placement of the variable retarders (VR-A, VR-B, VR-C, and VR-Sig) for polarization control and the system for measuring the phase between the C and reference pulses. BS: beam splitter, M: mirror, CAM: CCD camera. Times τ and T are the delays between excitation pulses A-B and B-C respectively, τ_R is the reference-signal time delay, f is the focal length, and ϕ_{CR} is the measured phase between the C and reference pulses.

Optics EXPRESS

The QW sample is a chip cleaved from the same wafer as used in [13]. It was grown by molecular beam epitaxy (MBE) and consists of 4 periods of 10-nm GaAs wells with 10-nm $Al_{0.3}Ga_{0.7}As$ barriers. The chip is attached to a sapphire substrate and is thinned for transmission measurements. The MC sample was also grown by MBE on a GaAs substrate [14,17] to have mirrors consisting of GaAs/AlAs (14.5 and 12 bilayer) distributed Bragg reflectors separated by a wedged GaAs λ cavity, with a cavity mode near 830 nm. In the center of the cavity, at the antinode of its electric field, is a single 8-nm thick $In_{0.04}Ga_{0.96}As$ QW. Cavity detuning with respect to the QW exciton is adjusted by changing the position of the excited spot on the sample along the direction of the wedge.

Before presenting 2D spectra, we discuss details of the polarization control, phasing using STRA, reference phase measurement, and phase cycling.

2.1. Polarization control using liquid crystal variable retarders

Polarization control in 2DCS is typically accomplished using static waveplates [6,13]. A separate time scan is performed for each polarization configuration. Here, we instead use liquid crystal variable retarders to control the polarization. The placement of the VRs (Meadowlark LRC-100-IR1 [18]) in the experimental apparatus is depicted in Fig. 1. These produce a zero-order retardance that depends on the applied AC input voltage amplitude. The retardance of the VRs at a given input voltage depends on the laser central wavelength and the ambient temperature. We calibrate the VRs using a Wollaston prism and power meter to check the purity of the vertical and horizontal polarization states. An additional quarter waveplate is used before the polarizer to check the purity of the circular polarization states. The ratio of power in the desired polarization state and the opposite polarization state is measured to be >100.

Variable retarders are placed in the A, B, and C paths to control the polarization state of the three excitation pulses. A fourth retarder is placed in the outgoing FWM path, so that horizontal or circularly polarized FWM is converted to vertical polarization before being combined with the vertically polarized reference pulse and sent to the spectrometer. A polarizer before the spectrometer ensures that only vertical polarization is detected. The average power through each VR is typically less than 1 mW, which is orders of magnitude below their damage threshold.

In order to phase the spectra for an arbitrary polarization configuration, we need to calculate the phase shift imparted by the VRs. The refractive index along only one axis is affected when the voltage amplitude is changed; we verified this property using polarization-dependent spatial interferometry. The Jones matrix is, for a retardance Γ,

$$L_\Gamma = \begin{pmatrix} e^{i\Gamma} & 0 \\ 0 & 1 \end{pmatrix}, \tag{1}$$

for a VR oriented with its fast axis along the x (vertical) direction. The VRs for polarization control are oriented with their fast axis at 45° with respect to the vertical axis, so the Jones matrix is

$$P_\Gamma^{\pm} = R(\pm 45^\circ) L_\Gamma R(\mp 45^\circ) = \frac{1}{2}\begin{pmatrix} e^{i\Gamma}+1 & \mp e^{i\Gamma} \pm 1 \\ \mp e^{i\Gamma} \pm 1 & e^{i\Gamma}+1 \end{pmatrix}, \tag{2}$$

where R(θ) is a rotation matrix.

We are concerned only with vertical and horizontal linear polarization (V and H respectively) and right and left circular polarization (σ^+ and σ^- respectively). A half wave plate has $\Gamma = \pi$, and a quarter wave plate has $\Gamma = \pi/2$. From Eq. (2) we calculate that, for a VR oriented at −45° with initially vertically (V) polarized light, the polarization state at the output is $e^{i\pi/4}\sigma^+$ for $\Gamma = \pi/4$, $e^{i\pi}H$ for $\Gamma = \pi/2$, and $e^{i\pi/4}\sigma^-$ for $\Gamma = 3\pi/4$. Here we have calculated the phase shift of the light

Optics EXPRESS

with respect to $\Gamma = 0$ (V polarization). That is, the A, B, and C VRs produce an additional $\pi/4$, π, and $\pi/4$ phase shift when producing σ^+, H, and σ^- polarized light respectively.

2.2. Phasing the 2D spectrum

Phasing the 2D spectrum is straightforward when all pulses are polarized the same way, as a slice projection of the 2D spectrum then corresponds to an easily measured transient-absorption spectrum [1]. For the co-linear polarization configuration (all pulses vertically polarized), we use the tracer as the probe in a measurement of the SRTA, with the combined A and B pulses as the pump. We use two pulses for the pump in order to match the total power on the sample during the 2D scan, since the lineshape can depend sensitively on power [19]. The nonlinear polarization that generates differential absorption of the tracer is, to third-order in the field,

$$P_{SRTA}(\omega) = \chi^{(3)} E_B^*(\omega) E_B(\omega) E_T(\omega) + \chi^{(3)} E_A^*(\omega) E_A(\omega) E_T(\omega). \tag{3}$$

where E_B, E_A, and E_T are the electric fields of the B, A, and tracer pulses, respectively. The electric field E_{SRTA} radiated by this polarization combines with the tracer pulse to produce the differential absorption spectrum,

$$S_r(\omega) = I_T(\omega) - I_{T,0}(\omega) \propto \mathrm{Re}\{E_T^*(\omega) E_{SRTA}(\omega)\}, \tag{4}$$

where $I_T(\omega)$ ($I_{T,0}(\omega)$) is the tracer spectrum with (without) the pump.

This can be used to phase the 2D spectrum because, if the fields B, A, and T are the same magnitude and relative timing as the A, B, and C fields for the zeroth step of the 2D scan, $P_{SRTA}(\omega)$ in Eq. (3) is exactly the same as the nonlinear polarization that produces the 2D spectrum,

$$P_{FWM}(\omega) = \chi^{(3)} E_A^*(\omega) E_B(\omega) E_C(\omega), \tag{5}$$

for the first step in the 2D scan, except that the phases of pulses B and C cancel in Eq. (3) because each term contains the field multiplied by its complex conjugate. The phase in Eq. (4) from the two terms in Eq. (3) goes as $-\phi_B + \phi_B + \phi_T - \phi_T = 0$ and $-\phi_A + \phi_A + \phi_T - \phi_T = 0$. The corresponding spectral interferogram, measured at each time step to construct the 2D spectrum, is

$$S(\omega) \propto \mathrm{Re}\left\{E_R^*(\omega) E_{FWM}(\omega) e^{i\phi_R}\right\}, \tag{6}$$

where $E_R(\omega)$ is the reference field. The phase of this signal goes as $-\phi_A + \phi_B + \phi_C - \phi_R$. The reference pulse precedes the FWM field by a fixed delay τ_R that is found by spectral interferometry of the reference and tracer pulses. This fixed delay produces an additional phase term $e^{i\omega\tau_R}$ that is used in the extraction of $E_{FWM}(\omega)$.

To find ϕ_R, we replace E_{SRTA} in Eq. (4) with $E_{FWM} e^{i\phi_R}$ and approximate the tracer field as having a flat phase, i.e. $E_T(\omega) \propto \sqrt{I_T(\omega)}$, yielding

$$S_f(\omega) = \mathrm{Re}\left\{\sqrt{I_T(\omega)} E_{FWM}(\omega) e^{i\phi_R}\right\}. \tag{7}$$

We fit $S_f(\omega)$ to the measured SRTA spectrum $S_r(\omega)$ to find the best value of ϕ_R and then use that value at each subsequent step in the 2D scan to find the extracted FWM field using Eq. (6). The SRTA results and best fit of the initial FWM signal are shown in Fig. 2. For both samples, the SRTA spectrum is reasonably well fit to Eq. (7) with a single fitting parameter ϕ_R.

We specify the polarization configuration using the notation $ABCF$, which gives the polarization of the A, B, and C pulses, and the polarization of the FWM emission, respectively. The first polarization configuration measured is always VVVV. At the beginning of every scan, the tracer spectrum is measured with and without the A and B pulses blocked so that we can construct the SRTA spectrum. This process is fully automated; beams are blocked and unblocked by

Optics EXPRESS

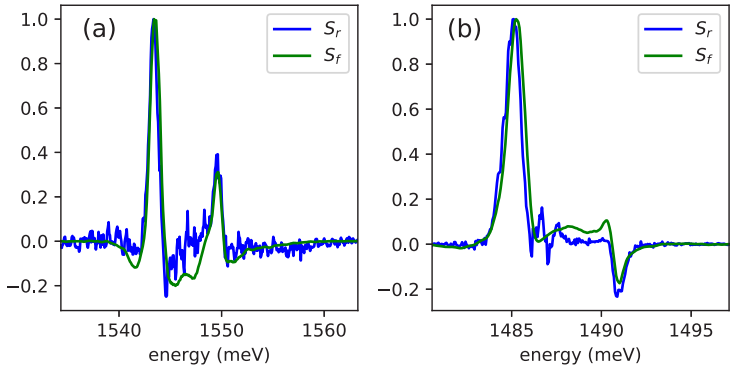

Fig. 2. Spectrally-resolved transient absorption (SRTA, blue) [Eq. (4)] and phased extracted FWM spectrum (green) [Eq. (7)] for VVVV polarization in (a) a four-period GaAs/AlGaAs quantum well sample and (b) a InGaAs/GaAs quantum well sample embedded in a microcavity for $\Delta = -6.0$ meV.

shutters created from inexpensive servos. The phase ϕ_R for the *VVVV* case is found by the fitting procedure just described and then applied to the rest of the polarization configurations, accounting for the polarization dependent phase shift produced by the variable retarder in each beam. The calculated phase offsets for each polarization configuration are shown in Table 1 below for commonly used polarization states VHHV (cross linear), $\sigma^+\sigma^+\sigma^+\sigma^+$ (co-circular), and $\sigma^-\sigma^-\sigma^+\sigma^+$ (cross-circular). The total phase $\phi_{tot} = -\phi_A + \phi_B + \phi_C + \phi_{FWM}$ is the offset that has to be added to ϕ_R in order to phase the spectrum.

Table 1. Summary of phase shift due to each variable retarder and the total phase shift ϕ_{tot} applied to each FWM spectrum during the 2D scan. The quantity in the last column, ϕ_{CR}, gives the phase shift due to the auxiliary reference phase measurement, which is discussed in Section 2.3.

A	B	C	FWM	$-\phi_A + \phi_B + \phi_C$	ϕ_{FWM}	ϕ_{tot}	ϕ_{CR}
V	H	H	V	$0 + \pi/2 + \pi/2$	0	π	0
σ^+	σ^+	σ^+	σ^+	$-\pi/4 + \pi/4 + \pi/4$	$\pi/4$	$\pi/2$	$-\pi/2$
σ^-	σ^-	σ^+	σ^+	$\pi/4 - \pi/4 + \pi/4$	$\pi/4$	$\pi/2$	$-\pi/2$

2.3. Reference phase measurement

To properly track the evolving phase of the FWM as a function of time delay, we require phase stability among all four pulses. The relative phase between the *A*, *B*, *C*, and tracer/reference pulses is locked inside the MONSTR by three feedback loops. The *A*, *B*, and *C* pulses are focused by a single lens and remain phase stable after exiting the MONSTR. However, the reference propagates around the sample and recombines with the FWM, forming a free space interferometer with an additional phase ambiguity. The reference pulse thus picks up a phase shift with respect to the excitation pulses due to thermal changes and air currents. As is done in previous work [15], we measure this phase drift by interfering the reference with the transmitted *C* pulse. In our experiment, *C* goes through the variable retarder, producing a polarization-dependent phase. This prevented us from using this measurement to actively lock the phase [15], because the sudden change in phase during a transition from one polarization to the next disrupts the feedback loop.

Instead, we record an interferogram using an auxiliary camera placed where the *C* and reference pulses cross [20]. We compensated for delay time between the two beams using a pair of glass wedges. Data acquisition of the auxiliary camera is triggered using the "fire" output of the spectroscopy camera, and the exposure time is set to match. We find unchanged fringe visibility

Optics EXPRESS

for exposure times from a few milliseconds up to 1 s, indicating minimal rapid phase jitter between the two pulses. In order to have good fringe visibility regardless of C polarization, we placed a linear polarizer at 45° in the outgoing C path.

An example interferogram measured using the auxiliary camera is shown in Fig. 3(a). The relative phase between the outgoing C and reference pulses is found from the interferogram by Fourier analysis. Figure 3(b) shows the typical phase evolution during a 160 step scan as green dots. The fringes are shifted because of the phase shift imparted on the C beam by the VR, but because of the presence of a 45° polarizer, this phase shift ϕ_{CR} is different from the phase shift discussed earlier. Using the same Jones matrix analysis discussed earlier, one can show that the C phase is changed by π for horizontal polarization and $-\pi/2$ for σ^+ polarization. These values agree with experimental results, as shown in blue and red in Fig. 3(b). This additional polarization-dependent phase ϕ_{CR} is included in the FWM phase correction at each time step of the 2D scan. For completeness, values of ϕ_{CR} are given for each polarization configuration in Table 1.

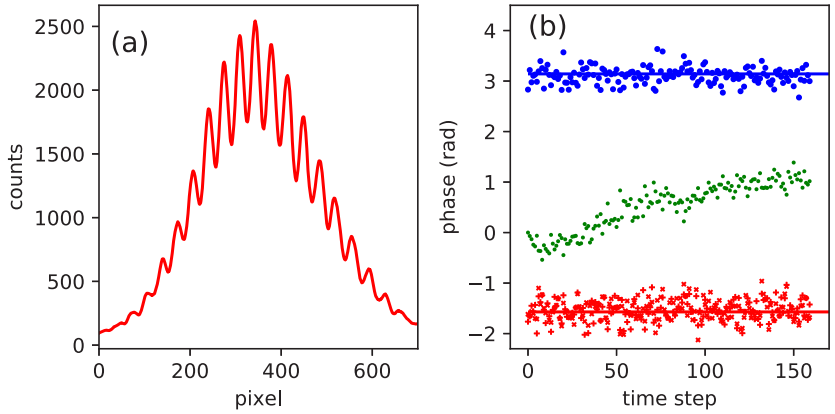

Fig. 3. Reference phase correction. (a) Typical interferogram from which the relative phase between the C and reference pulses phase is found. (b) Phase as a function of shot number for a 2D scan. The phase shift of the *VVVV* polarization is shown in green. The relative phase shift between *VVVV* and *VHHV* is shown in blue, and the relative phase shift between *VVVV* and $\sigma^+\sigma^+\sigma^+\sigma^+$ is shown in red. Blue and red horizontal lines show the theoretical values π and $-\pi/2$.

2.4. Phase cycling

Finally, phase cycling [10] removes artifacts caused by scattered light and improves the signal to noise ratio. In our apparatus this is done using two additional liquid crystal variable retarders in the A and B paths before the polarization optics. These are placed before the A and B polarization controlling variable retarders with the fast axis along the vertical axis, so that an additional phase ϕ can be imparted on each pulse without affecting its polarization. At each step and polarization, spectra are recorded for $\phi_A \in (0, \pi)$ and $\phi_B \in (0, \pi)$. The phase-cycled FWM signal is the combination $S_{00} - S_{0\pi} - S_{\pi 0} + S_{\pi\pi}$, where S_{AB} is the measured FWM/reference interferogram at a particular phase for pulses A and B. Scattered light from pulses A, B, and C is subtracted out by this procedure, and it also isolates the interference fringes between the reference and the FWM from the non-oscillating spectral background.

Optics EXPRESS

3. Two-dimensional spectroscopy results and discussion

Scans were performed with a step size of 49 HeNe fringes, corresponding to 52 fs. This step size was chosen because with 49 times undersampling, the 2D spectrum is folded cleanly into the middle of a Nyquist window. In order to ensure that the scan started at $\tau = 0$, we performed interferometric cross correlations using a camera imaging a replica of the focal plane [15]. Scans were done with the rephasing time ordering, with a mixing time of $T = 120$ fs. Note that in all following spectra the absorption photon energy is shown in the negative frequency space, consistent with the numerical assignment of the emission spectrometer reading positive photon energy and the phase-matching condition with the conjugated A pulse arriving first.

Before showing results, we note that reduced acquisition time is an important benefit of variable retarder based polarization control and phase cycling. A 49 fringe step takes 9 seconds, including stage settling time and re-locking the feedback loop. For a scan with 200 ms exposure time, 4 state phase cycling, and 100 steps, a scan for a single polarization takes about 19 minutes. Changing the polarization requires only 25 ms, so if we capture four polarizations in a single scan using our scheme, a scan takes 30 minutes. This is a speedup of a factor of 2.5 over 4 separate scans, not including the time required to manually change the polarization using static waveplates.

3.1. Four-period quantum well

First we reproduce polarization-dependent 2D spectra using a sample from the same wafer as used in a previous experiment [13]. The sample was held at 10 K, and we use 600 μW average power per beam. Example 2D spectra are shown in Fig. 4. The top row shows the magnitude of the normalized 2D spectrum for each polarization configuration. The bottom row shows the real part, normalized to the maximum value of the corresponding magnitude plot.

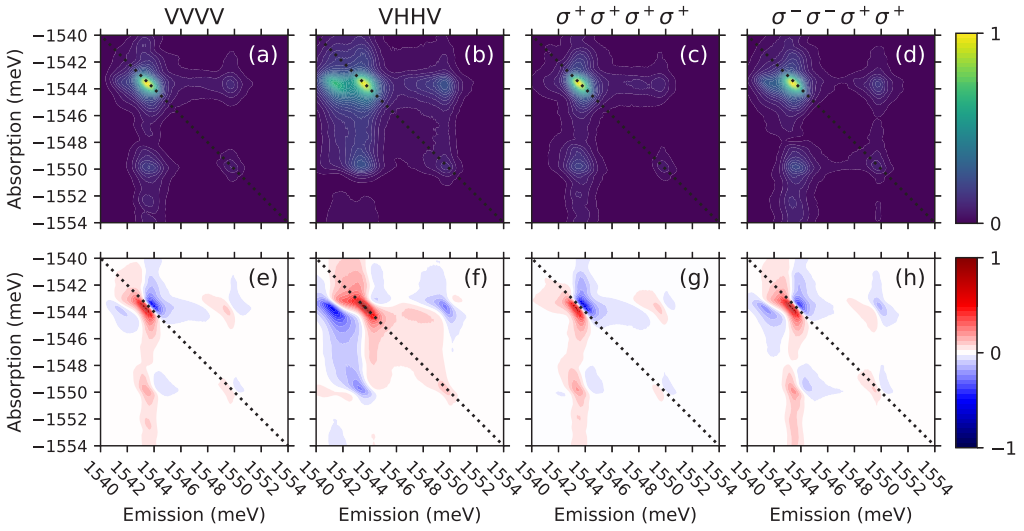

Fig. 4. Polarization dependent two-dimensional spectra for four-period QW. (a-d) Absolute value of the 2D spectrum for (a) co-linear, (b) cross-linear, (c) co-circular, and (d) cross-circular polarization. (e-h) Real part of the complex 2D spectrum for (e) co-linear, (f) cross-linear, (g) co-circular, and (h) cross-circular polarization. The peak in the upper left corresponds to the heavy hole exciton. Its polarization-dependent lineshape is consistent with previous results (cf. Figure 3 of [13])

Optics EXPRESS

The results show four main features: the heavy-hole exciton (strong on the diagonal at −1543 meV, 1543 meV), the light-hole exciton (weaker on the diagonal at −1550 meV, 1550 meV) and two off-diagonal features indicative of quantum coherence between the excitons during delay τ and Raman-like coherences during mixing time T [21,22]. In addition a heavy-hole biexciton is seen shifted along the emission axis from the heavy-hole exciton in all polarization cases other than the co-circular configuration. The polarization-dependent lineshape of the features generally agree with previous results [13], which is evidence that the phasing procedure described earlier works for all polarization configurations. Most importantly, the strongest feature, due to the heavy-hole exciton, has a dispersive lineshape in the antidiagonal direction for VVVV, $\sigma^+\sigma^+\sigma^+\sigma^+$, and $\sigma^-\sigma^-\sigma^+\sigma^+$ and a positive (pure absorptive) lineshape for VHHV, as observed previously [13]. The smaller energy separation between heavy- and light-hole excitons is attributed to a lower strain or weaker quantum confinement and the narrower width along the diagonal is attributed to less inhomogeneous broadening arising from well width disorder over the spot size or excitation-induced effects [3,23]. The weaker cross peaks relative to Fig. 3 of [13] is attributed to the different tuning of the laser spectrum with respect to the exciton lines and weaker light-hole exciton absorption with respect to the heavy-hole exciton [6].

3.2. Quantum well in microcavity

Next we studied a QW embedded in resonant MCs, where comparable absolute 2D spectra have been published [14,24,25], but phased spectra have not. Previous work has focused on measuring the polarization dependence to examine many-body interactions at fixed values of detuning Δ and examining one- and two-quantum spectra [24,25]. A Δ-dependence for linear polarization has also been published, revealing an interplay between exciton-polaritons and biexciton states [14]. Finally, in-plane wavevector dispersion has been investigated to understand polariton-polariton interactions [25].

Figure 5 shows the polarization dependence of the rephasing one-quantum 2D spectra for $\Delta = -6.0$ meV and with the axis of the focused excitation box at normal incidence to the MC. At this detuning, the lower polariton (on the diagonal at −1486 meV, 1486 meV) is mostly light-like and the upper polariton (on the diagonal at −1491 meV, 1491 meV) is mostly exciton-like. Because of the strong absorption of light in the microcavity, the all-optical phasing technique [12], which is the only other way we know of to phase arbitrarily polarized spectra, proved impossible to implement. The variable retarder based technique can because phasing is done through SRTA for one polarization configuration and then applied to all the others.

Based on previous measurements of excitons in GaAs [26], it is expected that at least the upper polariton feature should have a dispersive lineshape in the antidiagonal direction, as in the quantum well sample discussed in the previous section. In addition, there are two off-diagonal features presumably associated with quantum coherence between the two polariton branches, since they share a common ground state. A final feature is laterally shifted along the emission axis from the upper-polariton (at −1491 meV, 1489 meV) and is attributed to a biexciton resonance with an appropriate binding energy for this system [14]. Interestingly, the phase of the biexciton response, which is negative in the QW sample, is somewhat dispersive in the microcavity. At this detuning there may still be weak interactions between the cavity and all material resonances [14]. However, the assignment of the phase in the microcavity data should be considered preliminary. The fact that the lineshape of the exciton-like polariton branch at negative detuning is similar to the exciton in a bare quantum well makes physical sense and gives us confidence in the assignment of the phase, but more work is needed to confirm our results. In samples with high optical density, propagation effects must be carefully considered [27,28].

Optics EXPRESS

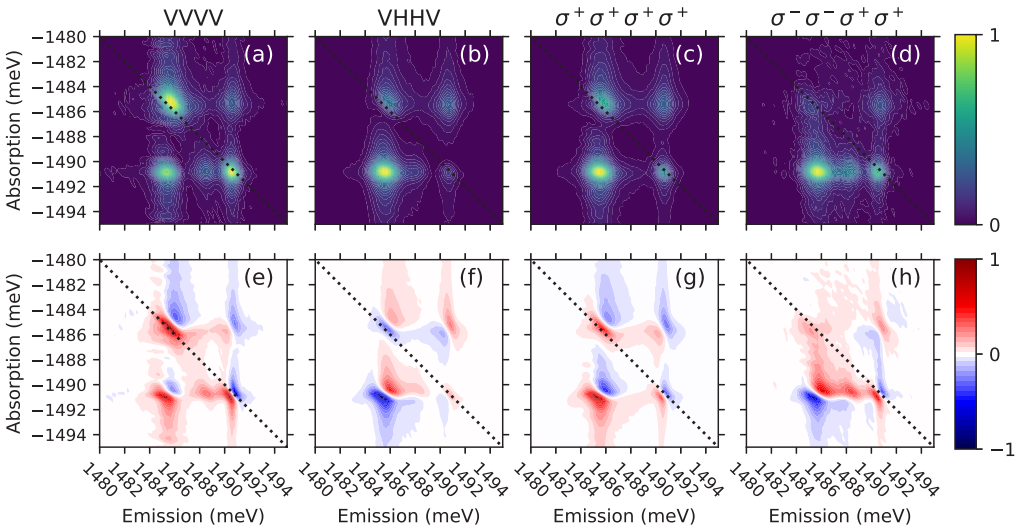

Fig. 5. Polarization dependent two-dimensional spectra for a single QW embedded in a MC for a detuning parameter of $\Delta = -6$ meV. (a-d) Absolute value of the 2D spectrum for (a) co-linear, (b) cross-linear, (c) co-circular, and (d) cross-circular polarization. (e-h) Real part of the complex 2D spectrum for (e) co-linear, (f) cross-linear, (g) co-circular, and (h) cross-circular polarization.

4. Conclusion

In summary, we have demonstrated a system capable of capturing multiple polarization-dependent 2D coherent spectra in a single scan of the delay stages. Using variable retarders for polarization control enables phasing of spectra from multiple polarization configurations using a single SRTA measurement. In addition, by placing the faster polarization control loop within the slow delay scanning loop we have increased the data acquisition time by approximately a factor of 3. Our demonstration with a previously studied thin multiple quantum well is important for validation of the method, while its extension to the microcavity sample, where phasing for non-collinear polarization combinations was not possible, shows the important capability of the method.

Funding

National Institute of Standards and Technology (Scientific and Technical Research and Services).

Acknowledgments

We thank E. J. Heilweil and L. Lu for technical assistance. G.M.W. was supported by the NIST Summer Undergraduate Research Fellowship program.

References

1. D. M. Jonas, "Two-dimensional femtosecond spectroscopy," Annu. Rev. Phys. Chem. **54**(1), 425–463 (2003).
2. G. Moody, M. Siemens, A. Bristow, X. Dai, D. Karaiskaj, A. Bracker, D. Gammon, and S. Cundiff, "Spectral broadening and population relaxation in a GaAs interfacial quantum dot ensemble and quantum well nanostructure," Phys. Status Solidi B **248**(4), 829–832 (2011).
3. A. D. Bristow, T. Zhang, M. E. Siemens, S. T. Cundiff, and R. P. Mirin, "Separating homogeneous and inhomogeneous line widths of heavy- and light-hole excitons in weakly disordered semiconductor quantum wells," J. Phys. Chem. B **115**(18), 5365–5371 (2011).
4. Y. D. Glinka, Z. Sun, M. Erementchouk, M. N. Leuenberger, A. D. Bristow, S. T. Cundiff, A. S. Bracker, and X. Li, "Coherent coupling between exciton resonances governed by the disorder potential," Phys. Rev. B **88**(7), 075316 (2013).

Optics EXPRESS

5. B. L. Wilmer, D. Webber, J. M. Ashley, K. C. Hall, and A. D. Bristow, "Role of strain on the coherent properties of GaAs excitons and biexcitons," Phys. Rev. B **94**(7), 075207 (2016).
6. T. Zhang, I. Kuznetsova, T. Meier, X. Li, R. P. Mirin, P. Thomas, and S. T. Cundiff, "Polarization-dependent optical 2D Fourier transform spectroscopy of semiconductors," Proc. Natl. Acad. Sci. U. S. A. **104**(36), 14227–14232 (2007).
7. D. Karaiskaj, A. D. Bristow, L. Yang, X. Dai, R. P. Mirin, S. Mukamel, and S. T. Cundiff, "Two-quantum many-body coherences in two-dimensional Fourier-transform spectra of exciton resonances in semiconductor quantum wells," Phys. Rev. Lett. **104**(11), 117401 (2010).
8. D. B. Turner, P. Wen, D. H. Arias, K. A. Nelson, H. Li, G. Moody, M. E. Siemens, and S. T. Cundiff, "Persistent exciton-type many-body interactions in GaAs quantum wells measured using two-dimensional optical spectroscopy," Phys. Rev. B **85**(20), 201303 (2012).
9. G. Nardin, G. Moody, R. Singh, T. M. Autry, H. Li, F. Morier-Genoud, and S. T. Cundiff, "Coherent excitonic coupling in an asymmetric double InGaAs quantum well arises from many-body effects," Phys. Rev. Lett. **112**(4), 046402 (2014).
10. P. Tian, D. Keusters, Y. Suzaki, and W. S. Warren, "Femtosecond phase-coherent two-dimensional spectroscopy," Science **300**(5625), 1553–1555 (2003).
11. J. O. Tollerud and J. A. Davis, "Coherent multi-dimensional spectroscopy: Experimental considerations, direct comparisons and new capabilities," Prog. Quantum Electron. **55**, 1–34 (2017).
12. A. D. Bristow, D. Karaiskaj, X. Dai, and S. T. Cundiff, "All-optical retrieval of the global phase for two-dimensional Fourier-transform spectroscopy," Opt. Express **16**(22), 18017–18027 (2008).
13. A. D. Bristow, D. Karaiskaj, X. Dai, R. P. Mirin, and S. T. Cundiff, "Polarization dependence of semiconductor exciton and biexciton contributions to phase-resolved optical two-dimensional Fourier-transform spectra," Phys. Rev. B **79**(16), 161305 (2009).
14. B. L. Wilmer, F. Passmann, M. Gehl, G. Khitrova, and A. D. Bristow, "Multidimensional coherent spectroscopy of a semiconductor microcavity," Phys. Rev. B **91**(20), 201304 (2015).
15. A. D. Bristow, D. Karaiskaj, X. Dai, T. Zhang, C. Carlsson, K. R. Hagen, R. Jimenez, and S. T. Cundiff, "A versatile ultrastable platform for optical multidimensional Fourier-transform spectroscopy," Rev. Sci. Instrum. **80**(7), 073108 (2009).
16. L. Lepetit, G. Chériaux, and M. Joffre, "Linear techniques of phase measurement by femtosecond spectral interferometry for applications in spectroscopy," J. Opt. Soc. Am. B **12**(12), 2467–2474 (1995).
17. G. Khitrova, H. Gibbs, F. Jahnke, M. Kira, and S. Koch, "Nonlinear optics of normal-mode-coupling semiconductor microcavities," Rev. Mod. Phys. **71**(5), 1591–1639 (1999).
18. Certain commercial equipment, instruments, or materials are identified in this paper in order to specify the experimental procedure adequately. Such identification is not intended to imply recommendation or endorsement by the National Institute of Standards and Technology, nor is it intended to imply that the materials or equipment identified are necessarily the best available for the purpose.
19. J. Tollerud and J. A. Davis, "Two-dimensional double-quantum spectroscopy: peak shapes as a sensitive probe of carrier interactions in quantum wells," J. Opt. Soc. Am. B **33**(7), C108–C114 (2016).
20. E. Backus, S. Garrett-Roe, and P. Hamm, "Phasing problem of heterodyne-detected two-dimensional infrared spectroscopy," Opt. Lett. **33**(22), 2665–2667 (2008).
21. L. Yang, I. V. Schweigert, S. T. Cundiff, and S. Mukamel, "Two-dimensional optical spectroscopy of excitons in semiconductor quantum wells: Liouville-space pathway analysis," Phys. Rev. B **75**(12), 125302 (2007).
22. L. Yang, T. Zhang, A. D. Bristow, S. T. Cundiff, and S. Mukamel, "Isolating excitonic Raman coherence in semiconductors using two-dimensional correlation spectroscopy," J. Chem. Phys. **129**(23), 234711 (2008).
23. X. Li, T. Zhang, C. N. Borca, and S. T. Cundiff, "Many-body interactions in semiconductors probed by optical two-dimensional Fourier transform spectroscopy," Phys. Rev. Lett. **96**(5), 057406 (2006).
24. P. Wen, G. Christmann, J. J. Baumberg, and K. A. Nelson, "Influence of multi-exciton correlations on nonlinear polariton dynamics in semiconductor microcavities," New J. Phys. **15**(2), 025005 (2013).
25. N. Takemura, S. Trebaol, M. D. Anderson, V. Kohnle, Y. Léger, D. Y. Oberli, M. T. Portella-Oberli, and B. Deveaud, "Two-dimensional Fourier transform spectroscopy of exciton-polaritons and their interactions," Phys. Rev. B **92**(12), 125415 (2015).
26. T. H. Zhang, C. N. Borca, X. Q. Li, and S. T. Cundiff, "Optical two-dimensional Fourier transform spectroscopy with active interferometric stabilization," Opt. Express **13**(19), 7432–7441 (2005).
27. D. Keusters and W. S. Warren, "Propagation effects on the peak profile in two-dimensional optical photon echo spectroscopy," Chem. Phys. Lett. **383**(1-2), 21–24 (2004).
28. A. P. Spencer, H. Li, S. T. Cundiff, and D. M. Jonas, "Pulse propagation effects in optical 2D Fourier-transform spectroscopy: Theory," J. Phys. Chem. A **119**(17), 3936–3960 (2015).